Collective Instabilities and Halo Formation of Space-Charge Dominated Beams in a Particle-Beam Nonlinear-Dynamics Approach

K.Y. Ng, Fermilab* P.O. Box 500, Batavia, IL 60510

Abstract

Nonlinear dynamics deals with parametric resonances and diffusion, which are usually beam-intensity independent and rely on a particle Hamiltonian. Collective instabilities deal with beam coherent motion, where the Vlasov equation is frequently used in conjunction with a beam-intensity dependent Hamiltonian. We address the questions: Are the two descriptions the same? Are collective instabilities the results of encountering parametric resonances whose driving force is intensity dependent? The space-charge dominated beam governed by the Kapchinskij-Vladimirskij (K-V) envelope equation [1] is used as an example.

1 INTRODUCTION

Traditionally, the thresholds of collective instabilities are obtained by solving the Vlasov equation, the dynamics of which comes from the single-particle wakefield-dependent Hamiltonian. The Vlasov equation is often linearized so that the modes of collective motion can be described by a set of orthonormal eigenfunctions and their corresponding complex eigenvalues give the initial growth rates. The perturbation Hamiltonian ΔH_1 may have a time-independent component, for example, the space-charge self-field that determines the potential-well distortion of the unperturbed particle distribution, and the part involving the nonlinear magnetic fields, that gives rise to the dynamical aperture limitation. It may also have a time-dependent component, which includes the time-dependent effects of wakefields and produces coherent motion of beam particles. The harmonic content of the wakefields depends on the structure of accelerator components. If one of the resonant frequencies of the wakefields is equal to a fractional multiple of the unperturbed tune of unperturbed Hamiltonian H_0, a resonance is encountered. Depending on the stochasticity of the phase space, particles may be trapped into the resonant islands or diffuse towards resonant structures far away forming beam halos or getting lost. This may result in a runaway situation such that collective instability is induced.

Experimental measurements indicate that a small time dependent perturbation can create resonance islands in the longitudinal or transverse phase space and profoundly change the bunch structure [2]. For example, a modulating transverse dipole field close to the synchrotron frequency can split up a bunch into beamlets. Although these phenomena are driven by beam-intensity independent sources, they can also be driven by the space-charge force and/or the wakefields of the beam which are intensity dependent. Once perturbed, the new bunch structure can further enhance the wakefields inducing even more perturbation to the circulating beam. Experimental observation of hysteresis in collective beam instabilities seems to indicate that resonance islands have been generated by the wakefields.

For example, the Keil-Schnell criterion [3] of longitudinal microwave instability can be derived from the concept of bunching buckets, or islands, created by the perturbing wakefields. Particles in the beam will execute *synchrotron* motion inside these buckets leading to growth in the momentum spread of the beam. In fact, the collective growth rate is exactly equal to the angular synchrotron frequency inside these buckets. If the momentum spread of the beam is much larger than the bucket height, only a small fraction of the particles in the beam will be affected and collective instabilities will not occur. This mechanism has been called Landau damping.

As a result, we believe that the collective instabilities of a beam may also be tackled from a particle-beam nonlinear-dynamics approach, with collective instabilities occurring when the beam particles are either trapped in resonance islands or diffuse away from the beam core because of the existence of a sea of chaos. The advantage of the particle-beam nonlinear-dynamics approach is its ability to understand the hysteresis effects and to calculate the beam distribution beyond the threshold condition. Such a procedure may be able to unify our understanding of collective instabilities and nonlinear beam dynamics. Here, the stability issues of a space-charge dominated beam in a uniformly focusing channel are considered as an example [4].

2 ENVELOPE HAMILTONIAN

First, the envelope Hamiltonian is normalized to unit emittance and unit period. In terms of the normalized and dimensionless envelope radius R, together with its conjugate momentum P, the Hamiltonian for the beam envelope in a uniformly focusing channel can be written as [5, 6]

$$H_e = \frac{1}{4\pi}P^2 + V(R)\ , \tag{2.1}$$

$$V(R) = \frac{\mu^2}{4\pi}R^2 - \frac{\mu\kappa}{\pi}\ln\frac{R}{R_0} + \frac{1}{4\pi R^2}\ , \tag{2.2}$$

where $\mu/(2\pi)$ is the *unperturbed* particle tune, $\kappa = Nr_{\rm cl}/(\mu\beta^2\gamma^3)$ the *normalized* space-charge perveance, N the number of particles per unit length having classical radius $r_{\rm cl}$, and β and γ the relativistic factors of the beam. The normalized K-V equation then reads

$$\frac{d^2R}{d\theta^2} + \left(\frac{\mu}{2\pi}\right)^2 R = \frac{2\mu\kappa}{4\pi^2 R} + \frac{1}{4\pi^2R^3}\ . \tag{2.3}$$

The radius R_0 of the matched beam envelope or core occurs at the lowest point of the potential; i.e., $V'(R_0) = 0$, or

$$\mu R_0^2 = \sqrt{\kappa^2+1} + \kappa = \frac{1}{\sqrt{\kappa^2+1} - \kappa}\ . \tag{2.4}$$

From the second derivative of the potential, the small amplitude tune for envelope oscillations is therefore

* Operated by the Universities Research Association, under contracts with the US Department of Energy.

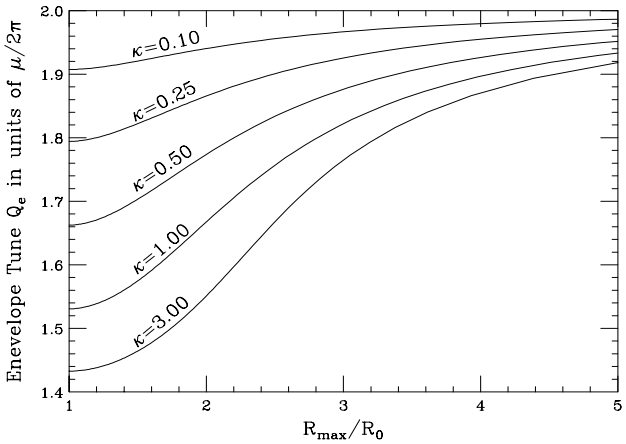

Figure 1: Envelope tune Q_e versus envelope mismatch $R_{\max}/R_0$ for various space-charge perveance κ. Notice that Q_e is represented by ν_e at $R_{\max}/R_0 = 1$ when the beam envelope is matched.

$$\nu_e = \frac{2\mu}{2\pi}\left[1-\kappa\left(\sqrt{\kappa^2+1}-\kappa\right)\right]^{1/2} \tag{2.5}$$

which approaches μ/π and $\sqrt{2}\mu/(2\pi)$ as κ approaches 0 and ∞, respectively.

For a mismatched beam, R varies between $R_{\min}$ and $R_{\max}$. To derive the tune of the mismatched envelope, it is best to go to the action-angle variables (J_e, ψ_e). The envelope tune and action are then

$$Q_e = \frac{dE_e}{dJ_e} = \nu_e + \alpha_e J_e + \cdots, \quad J_e = \frac{1}{2\pi}\oint P dR. \tag{2.6}$$

where E_e is the Hamiltonian value of the beam envelope, and the detuning α_e, defined by $H_e = \nu_e J_e + \frac{1}{2}\alpha_e J_e^2 + \cdots$, is computed to be

$$\alpha_e = \frac{3}{16\pi^3 R_0^4 \nu_e^2}\left[\mu\kappa + \frac{5}{R_0^2}\right] - \frac{5}{48\pi^5 R_0^6 \nu_e^4}\left[\mu\kappa + \frac{3}{R_0^2}\right]^2 + \cdots.$$

To obtain the envelope tune for large mismatch, one must compute numerically the action integral to obtain

$$Q_e = \frac{dE_e}{dJ_e} = 2\pi\left[\oint \frac{\partial P}{\partial E_e} dR\right]^{-1}, \tag{2.7}$$

The envelope tune is plotted in Fig. 1 as a function of the maximum envelope radius $R_{\max}$, which, for small mismatch, is related to the envelope action J_e by

$$R = R_0 + \left(\frac{J_e}{\pi\nu_e}\right)^{1/2}\cos Q_e\theta\,. \tag{2.8}$$

3 COLLECTIVE-MOTION APPROACH

Gluckstern, Cheng, Kurennoy, and Ye [7] have studied the collective beam stabilities of a space-charge dominated K-V beam in a uniformly focusing channel. The particle distribution f is separated into the unperturbed distribution f_0 and the perturbation f_1:

$$f(u, v, \dot{u}, \dot{v}\,; \theta) = f_0(u^2+v^2+\dot{u}^2+\dot{v}^2) + f_1(u, v, \dot{u}, \dot{v}\,; \theta)\,,$$

where u and v are the normalized transverse coordinates which are functions of the 'time' variable θ. Their derivatives with respect to time are denoted by $\dot{u}$ and $\dot{v}$. The unperturbed distribution,

$$f_0(u^2+v^2+\dot{u}^2+\dot{v}^2) = \frac{I_0}{v_0\pi^2}\delta(u^2+v^2+\dot{u}^2+\dot{v}^2-1)\,,$$

is the steady-state solution of the K-V equation (2.3) and is therefore time-independent. In the notation of Gluckstern, Cheng, Kurennoy, and Ye, I_0 is the average beam current and v_0 the longitudinal velocity of the beam particles. The perturbed distribution generates an electric potential G, which is given by the Poisson's equation

$$\nabla^2 G(u, v, \theta) = -\frac{1}{\epsilon_0}\int d\dot{u}\int d\dot{v} f_1(u, v, \dot{u}, \dot{v}\,; \theta)\,, \tag{3.1}$$

so that the Hill's equations in the two transverse planes become

$$\ddot{u} + u = -\frac{e\beta}{m_0 v_0^2 \epsilon}\frac{\partial G}{\partial u}\,, \quad \ddot{v} + v = -\frac{e\beta}{m_0 v_0^2 \epsilon}\frac{\partial G}{\partial v}\,, \tag{3.2}$$

where ϵ stands for the transverse emittance of the beam and m_0 the rest mass of the beam particle.

For small perturbation, the perturbation distribution is proportional to the derivative of the unperturbed distribution. This enables us to write

$$f_1(u, v, \dot{u}, \dot{v}; \theta) = g(u, v, \dot{u}, \dot{v}; \theta) f_0'(u^2+v^2+\dot{u}^2+\dot{v}^2)\,. \tag{3.3}$$

Substituting into the linearized Vlasov equation, we obtain

$$\frac{\partial g}{\partial\theta} + \dot{u}\frac{\partial g}{\partial u} + \dot{v}\frac{\partial g}{\partial v} - u\frac{\partial g}{\partial\dot{u}} - v\frac{\partial g}{\partial\dot{v}} = \frac{2e\beta}{m_0 v_0^2\epsilon}\left[\dot{u}\frac{\partial G}{\partial u} + \dot{v}\frac{\partial G}{\partial v}\right]. \tag{3.4}$$

Noting that the potential G is a polynomial, Gluckstern, *et. al.* are able to solve for g and G consistently in terms of hypergeometric functions. Thus a series of orthonormal eigenmodes are obtained for the perturbed distribution with their corresponding eigenfrequencies. These modes are characterized by (j, m), where j is the radial eigennumber and m the azimuthal eigennumber.

For the azimuthally symmetric $m = 0$ modes, (1,0) is the breathing mode of uniform density at a particular time while the (2,0) mode oscillates with a radial node between $R = 0$ and $R = R_0$ so that the density becomes nonuniform. The higher modes are similar, with mode $(j, 0)$ having $j-1$ radial nodes. When the eigenfrequency of a mode is complex, the mode becomes unstable with a collective growth rate. Stability is studied in terms of tune depression $\eta = \sqrt{\kappa^2+1}-\kappa$ and the amount of envelope mismatch. The former is defined as the ratio of the particle tune with space charge to the particle tune without space charge for a *matched* beam. Thus η ranges from 0 to 1; $\eta = 1$ implies zero space charge while $\eta = 0$ implies infinite space charge.

Gluckstern, *et. al.* showed that mode (1,0) is stable for any mismatch and tune depression. Mode (2,0) becomes unstable at zero mismatch when the tune depression $\eta < 1/\sqrt{17} = 0.2435$. It is also unstable when the mismatch is large. This is plotted in Fig. 2 with the stable regions of modes (2,0), (3,0), and (4,0) enclosed, respectively, by the solid, dashed, and dot-dashed curves, a reproduction of Ref. 4. These latter two modes become unstable at zero mismatch when the tune depressions are less than 0.3859 and 0.3985, respectively. They found that the modes become more unstable as the number of radial nodes increases. Among all the azimuthals, they noticed that the azimuthally symmetric modes ($m = 0$) are the most unstable.

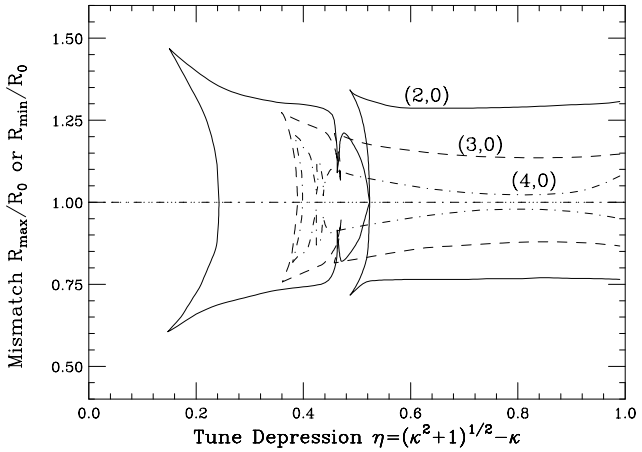

Figure 2: Beam stability plot versus particle tune depression η and beam envelope mismatch. The stability regions for modes (2,0), (3,0) and (4,0) are enclosed, respectively, by the solid, dashed, and dot-dashed curves. (Reproduced from Ref. 4).

4 PARTICLE-BEAM APPROACH

4.1 Particle Hamiltonian

We want to investigate whether the instability regions in the plane of tune depression and mismatch can be explained by nonlinear parametric resonances. First, let us study the transverse motion of a particle having zero angular momentum. The situation of finite momentum will be discussed later in Sec. 6. We choose y as the particle's transverse coordinate with canonical angular momentum p_y. Its motion is perturbed by an azimuthally symmetric oscillating beam core of radius R. The particle Hamiltonian is [6]

$$H_p = \frac{1}{4\pi}p_y^2 + \frac{\mu^2}{4\pi}y^2 - \frac{2\mu\kappa}{4\pi R^2}\,y^2\,\Theta(R-|y|) - \frac{2\mu\kappa}{4\pi}\left(1+2\ln\frac{|y|}{R}\right)\Theta(|y|-R)\,, \tag{4.1}$$

giving the equation of motion for y,

$$\frac{d^2y}{d\theta^2}+\left(\frac{\mu}{2\pi}\right)^2 y = \frac{\mu\kappa}{2\pi^2R^2}y\,\Theta(R-|y|)+\frac{\mu\kappa}{2\pi^2|y|}\,\Theta(|y|-R)\,. \tag{4.2}$$

For a weakly mismatched beam, the envelope radius is $R = R_0+\Delta R\cos Q_e\theta$. The particle Hamiltonian can also be expanded in terms of the equilibrium envelope radius R_0, resulting $H_p = H_{p0}+\Delta H_p$. The unperturbed Hamiltonian is

$$H_{p0} = \frac{1}{4\pi}p_y^2 + \frac{\mu^2}{4\pi}y^2 - \frac{2\mu\kappa}{4\pi R_0^2}\,y^2\,\Theta(R_0-|y|) - \frac{2\mu\kappa}{4\pi}\left(1+2\ln\frac{|y|}{R_0}\right)\Theta(|y|-R_0)\,, \tag{4.3}$$

and the perturbation

$$\Delta H_p \approx -\frac{\mu\kappa}{\pi R_0^2}\left[\frac{\Delta R}{R_0}(y^2-R_0^2) + \frac{3\Delta R^2}{2R_0^2}\left(y^2-\tfrac{1}{3}R_0^2\right)+\cdots\right]\Theta(R_0-|y|)\,. \tag{4.4}$$

Note that many non-contributing terms, like the ones involving the δ-function and δ'-function, have been dropped. Additionally, envelope oscillations do not perturb particle motion outside the envelope radius; thus the perturbing potential in Eq. (4.4) exists only inside the envelope.

For a matched beam, $\Delta H_p = 0$. Inside the core of uniform distribution, the particle motion is linear and its tune can be readily obtained:

$$\nu_p = \frac{\mu}{2\pi}\left(1-\frac{2\kappa}{\mu R_0^2}\right)^{1/2} = \frac{\mu}{2\pi}\left(\sqrt{\kappa^2+1}-\kappa\right)\,.$$

Thus, $\eta = \sqrt{\kappa^2+1}-\kappa$ is the tune depression.

When the particle spends time oscillating outside the beam envelope, its tune has to be computed numerically. First, the particle action is defined as

$$J_p = \frac{1}{2\pi}\oint p_y dy\,. \tag{4.5}$$

The particle tune Q_p is then given by

$$Q_p = \frac{dE_p}{dJ_p} = 2\pi\left[\oint\frac{\partial p_y}{\partial E_p}dy\right]^{-1}\,, \tag{4.6}$$

where E_p is the Hamiltonian value of the beam particle. The result is shown in Fig. 3 for various space-charge perveance κ. We see that when the particle motion is completely inside the beam envelope ($J_p < \frac{1}{2}$), the particle tune is a constant and is given by ν_p depending on κ only. As the particle spends more and more time outside the beam envelope, its tune increases because the space-charge force decreases as y^{-1} outside the envelope.

4.2 Particle Tune Inside a Mismatched Beam

To simplify the algebra, it is advisable to scale away the unperturbed particle tune $\mu/(2\pi)$ through the transformation: $\mu R^2 \to R^2$, $\mu y^2 \to y^2$, and $\mu\theta/(2\pi) \to \theta$. The envelope and particle equations become

$$\frac{d^2R}{d\theta^2}+R = \frac{2\kappa}{R}+\frac{1}{R^3}\,, \tag{4.7}$$

$$\frac{d^2y}{d\theta^2}+y-\frac{2\kappa}{R^2}y\,\Theta(R-|y|)-\frac{2\kappa}{y}\,\Theta(|y|-R)=0\,. \tag{4.8}$$

For one envelope oscillation period, the envelope radius R is periodic and Eq. (4.8) *inside* the envelope core becomes a Hill's equation with effective *field gradient* $K(\theta) = 1-2\kappa/R^2(\theta)$. The solution is then exactly the same as the Floquet transformation by choosing $y = aw(\theta)\cos[\psi(\theta)+\delta]$.

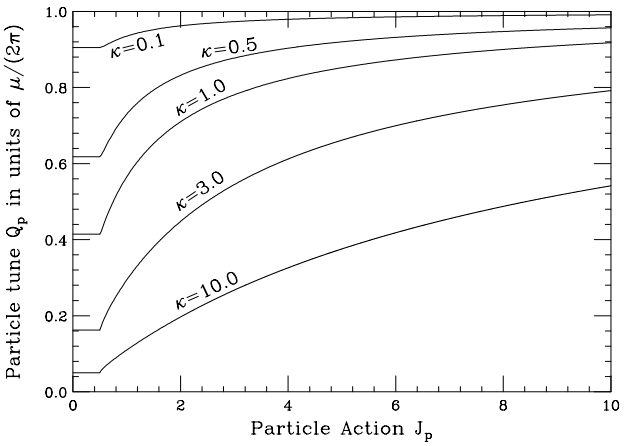

Figure 3: Particle tune Q_p as function of particle action J_p and space-charge perveance κ for a matched beam.

It is easy to show that the differential equation for w is exactly the envelope equation of Eq. (4.7). Thus we can replace w by R, and R^2 becomes the effective *betatron function*. Since the particle makes Q_p/Q_e betatron oscillations during one envelope fluctuation period, where Q_p is the particle tune, we have

$$\frac{Q_p}{Q_e} = \frac{\Delta\psi}{2\pi} = \frac{1}{2\pi}\oint \frac{d\theta}{R^2(\theta)} \,. \tag{4.9}$$

In Floquet's notation, with $\hat{y} = y/R$, Eq. (4.2) describing the motion of a particle modulated by a beam envelope becomes

$$\frac{d^2\hat{y}}{d\psi^2} + \hat{y} + 2\kappa R^2 \left[\frac{\hat{y}^2-1}{\hat{y}}\right] \Theta\left(|\hat{y}|-1\right) = 0 \,. \tag{4.10}$$

Thus, all particles inside the beam envelope have a fixed tune depending on the amount of space charge and envelope mismatch. Particles spending part of the time outside the beam envelope will have larger tunes. The Floquet transformation can also be accomplished by a canonical transformation employing the generating function

$$F_2(y,\hat{p}_y;\theta) = \frac{y\hat{p}_y}{R(\theta)} + \frac{yR'(\theta)}{2R(\theta)} \,, \tag{4.11}$$

where the prime denotes derivative with respect to θ. The new Hamiltonian in the Floquet coordinates becomes

$$\hat{H}_p(\hat{y},\hat{p}_y;\theta) = \frac{1}{R^2(\theta)}(\hat{y}^2+\hat{p}_y^2) + \kappa(\hat{y}^2 - \ln\hat{y}^2)\,\Theta(|\hat{y}|-1) \,. \tag{4.12}$$

For a small mismatch core fluctuation, we can write $R = R_0(1-M\cos Q_e\theta)$, where M can be interpreted as the mismatch parameter. The integral in Eq. (4.9) can be performed analytically to give

$$Q_p = \frac{\nu_p}{(1-M^2)^{3/2}} \,, \tag{4.13}$$

where $\nu_p = R_0^{-2} = \sqrt{\kappa^2+1} - \kappa$ is the particle tune when the envelope is matched. The analytic formula of Eq. (4.13), however, is only valid when the mismatch parameter $M \lesssim 0.2$. The reason is that the envelope equation is nonlinear in the presence of space charge. In other words, while minimum envelope radius is given by $R_{\min} = (1-M)R_0$, the maximum envelope radius is always $R_{\max} > (1+M)R_0$. In fact, when $M \to 1$, $R_{\min} \to 0$, but $R_{\max} \to \infty$. This can be seen in top plot of Fig. 4 with $(R_{\max}-R_0)/R_0$ versus $M = (R_0 - R_{\max})/R_0$. If the envelope oscillations were symmetric about R_0, the plot would follow the 45° dashed line instead. We see that the deviation is large when the mismatch and tune depression are large. When the approximation $R = R_0(1-M\cos Q_e\theta)$ breaks down, the particle tune can still be easily evaluated by performing the integral in Eq. (4.9) numerically. The lower plot of Fig. 4 shows the deviation of the actual particle tune Q_p from its analytic formula of Eq. (4.13).

5 PARAMETRIC RESONANCES

Particle motion is modulated by the oscillating beam envelope. Therefore, to study the resonance effect, we need to include the perturbation part ΔH_p of the particle Hamiltonian. We expand it as a Fourier series in the angle variable ψ_p yielding, for example,

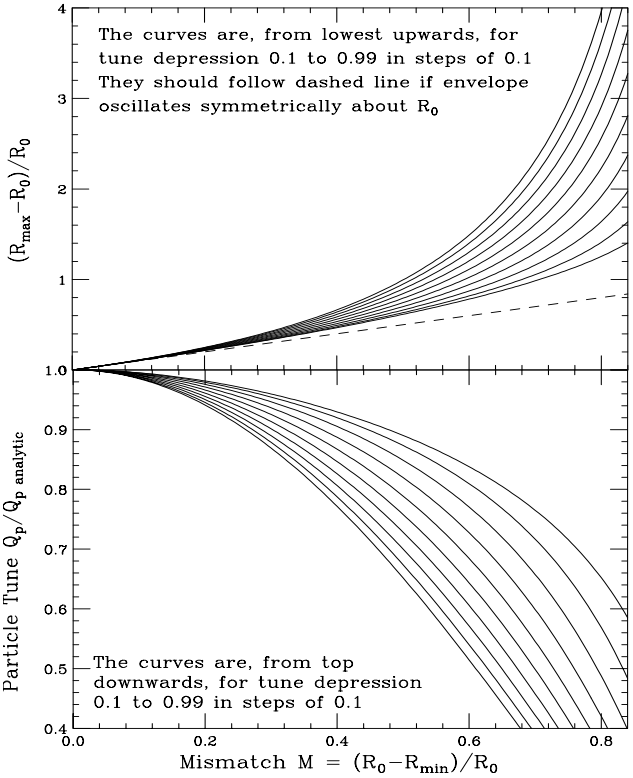

Figure 4: Top: $(R_{\max}-R_0)/R_0$ vs $M = (R_0-R_{\max})/R_0$ showing the large asymmetric envelope oscillation about the equilibrium radius R_0 when both the mismatch and tune depression are large. Bottom: Deviation of the actual particle tune Q_p from the value given Eq. (4.13) in the presence of mismatch.

$$(y^2 - R_0^2)\,\Theta(R_0-|y|) = \sum_{n=-\infty}^{\infty} G_n(J_p)e^{in\psi_p} \,. \tag{5.1}$$

Since ΔH_p is even in y, only even n harmonics survive. The particle Hamiltonian then becomes

$$H_p = H_{p0} + \frac{\mu\kappa}{2\pi R_0^2}\sum_{m=1}^{\infty}\sum_{\substack{n>0\\ \text{even}}}(m+1)M^m|G_{nm}| \times \times \sum_{i=\pm1}\cos(n\psi_p + imQ_e\theta + \gamma_n) + \cdots \,, \tag{5.2}$$

where γ_n are some phases and use has been made of $R = R_0(1-M\cos Q_e\theta)$, the approximation for small mismatch.

Focusing on the n:m resonance, a canonical transformation to the resonance rotating frame (I_p,ϕ_p) gives

$$\langle H_p\rangle = E_p(I_p) - \frac{m}{n}Q_eI_p + h_{nm}(I_p)\cos n\phi_p \,, \tag{5.3}$$

with the effective κ-dependent resonance strength

$$h_{nm} = \frac{(m+1)M^m\mu\kappa}{2\pi R_0^2}\,|G_{nm}(I_p)| \,. \tag{5.4}$$

As usual, there are n stable and n unstable fixed points which can be found easily. Since ΔH_p is a polynomial up to y^2 only and $y \propto \sin\psi_p$, we have, inside the envelope,

$$G_{nm} = \frac{1}{4\pi Q_e}J_p\delta_{n2} \,, \tag{5.5}$$

implying that only 2:m resonances are possible. Outside the envelope the resonance driving strengths can also be computed, and are plotted in Fig. 5. We see that although the

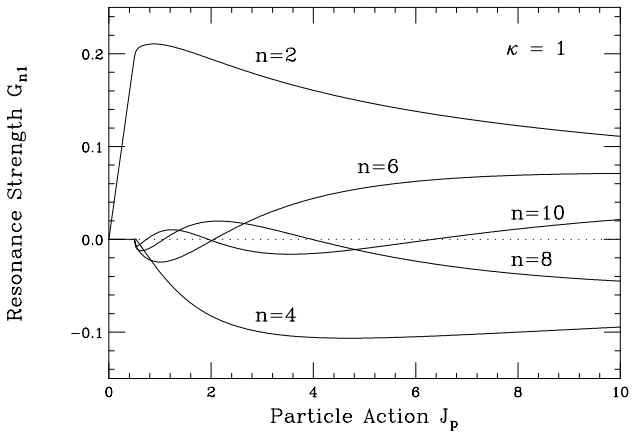

Figure 5: Plot of driving strengths of first-order resonances G_{n1} versus particle action J_p. Inside the envelope ($J_p < \frac{1}{2}$), only G_{21} is nonzero. Once outside the envelope, however, $|G_{n1}|$ for $n \geq 2$ increases rapidly from zero.

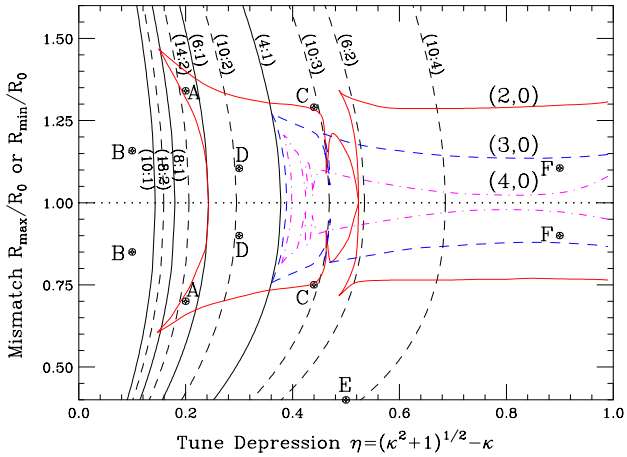

Figure 6: Plot of parametric resonance locations in the plane of tune-depression and beam envelope mismatch. First-order resonances are shown as solid while second- and higher-order resonances as dashes. Overlaid on top are the instability boundaries of modes (2,0), (3,0), and (4,0) derived by Gluckstern, *et. al*.

driving strengths G_{n1} for $n > 2$ vanish inside the envelope ($J_p < \frac{1}{2}$), they increase rapidly once outside. Including noises of all types, particles inside the K-V beam envelope can leak out. This situation is particularly true when the particle tune is equal to a fractional multiple of the envelope tune. A small perturbation may drive particles outside the beam envelope. Once outside, because of the nonvanishing driving strengths, these particles may be trapped into resonance islands or diffuse into resonances farther away. Once trapped or diffused, they cannot wander back into the envelope core. As more and more envelope particles leak out, the core stabilization is lost and an instability occurs.

Our job is, therefore, to map out the location of parametric resonances in the plane of mismatch and tune depression. Because particles are affected only by resonances when they are just outside the envelope core, their tunes are essentially the tune inside the beam envelope. At zero mismatch, the threshold for the n:m resonance can therefore be derived by equating ν_p/ν_e to m/n. Thus

$$\frac{\nu_p}{\nu_e} = \frac{\sqrt{\kappa^2+1}-\kappa}{2\left[1-\kappa\left(\sqrt{\kappa^2+1}-\kappa\right)\right]^{1/2}} \leq \frac{m}{n}\,, \qquad (5.6)$$

or

$$\kappa \geq \frac{\left(\frac{n}{m}\right)^2-4}{\sqrt{8\left[\left(\frac{n}{m}\right)^2-2\right]}}\,. \qquad (5.7)$$

In particular, for the 6:1 resonance, $\kappa \geq 8/\sqrt{17} = 1.9403$, or the tune depression is $\eta \leq 1/\sqrt{17} = 0.2425$, which agrees with Gluckstern's instability threshold for mode (2,0).

For a mismatched beam, the threshold for the n:m resonance is obtained by equating Q_p/Q_e at that mismatch to m/n. These resonances are labeled in Fig. 6 in the plane of tune depression and mismatch. The locus of the 2:1 resonance is the vertical line $\eta = 1$. This is obvious, because at zero space charge the particle tune is exactly two times the envelope tune regardless of mismatch. Also, it is clear from Eq. (4.10) that there will not be any Mathieu instability or half-integer stop-band [8]. Thus it appears that the 2:1 resonance would not influence the stability of a space-charge dominated beam. This is, in fact, not true. The stable fixed points of the 2:1 resonance are usually far away from the beam envelope. Thus particles can diffuse towards the 2:1 resonance to form beam halo. As more and more particles continue to diffuse from the beam core into the 2:1 resonance, the beam becomes unstable.

Trackings have been performed for particles outside the envelope core using the fourth-order symplectic integration developed by Forest and Berz [9]. The Poincaré surface of section is shown in Fig. 7A for the situation $\eta = 0.20$ ($\kappa = 2.4$) and $M = 0.3$, corresponding to Points A in Fig. 6. The innermost torus is the beam envelope. The sections are taken every envelope oscillation period when the envelope radius is at a minimum. For each envelope oscillation period, 500 to more than 1000 time steps have been used. We see that as soon as particles diffuse outside the beam envelope, they will encounter the 6:1 resonance, which is bounded by tori. This explains the front stability boundary of Gluckstern's mode (2,0). Since the 4:1 resonance is a strong one, its locus explains the front stability boundaries of Gluckstern's (3,0) and (4,0) modes also.

The Poincaré surface of section corresponding to Points B of Fig. 6 with $\eta = 0.10$ ($\kappa = 4.95$) $M = 0.15$ is shown in Fig. 7B. This is a close-up view showing only the region near the beam envelope; the 2:1 resonance and its separatrices are not shown because they look similar to those depicted in Fig. 7A. We see resonances like 14:2, 8:1, 16:2, 9:1, 10:1, etc, which are so closely spaced that they overlap to form a chaotic region. Particles that diffuse outward from the beam envelope will wander easily towards the 2:1 resonance along its separatrix. This region, where $\eta \lesssim 0.2$, is therefore very unstable.

Figure 7C shows the close-up Poincaré surface of section of Points C in Fig. 6 with $\eta = 0.44$ ($\kappa = 0.916$) and $M = 0.25$. Here the particles see many parametric reso-

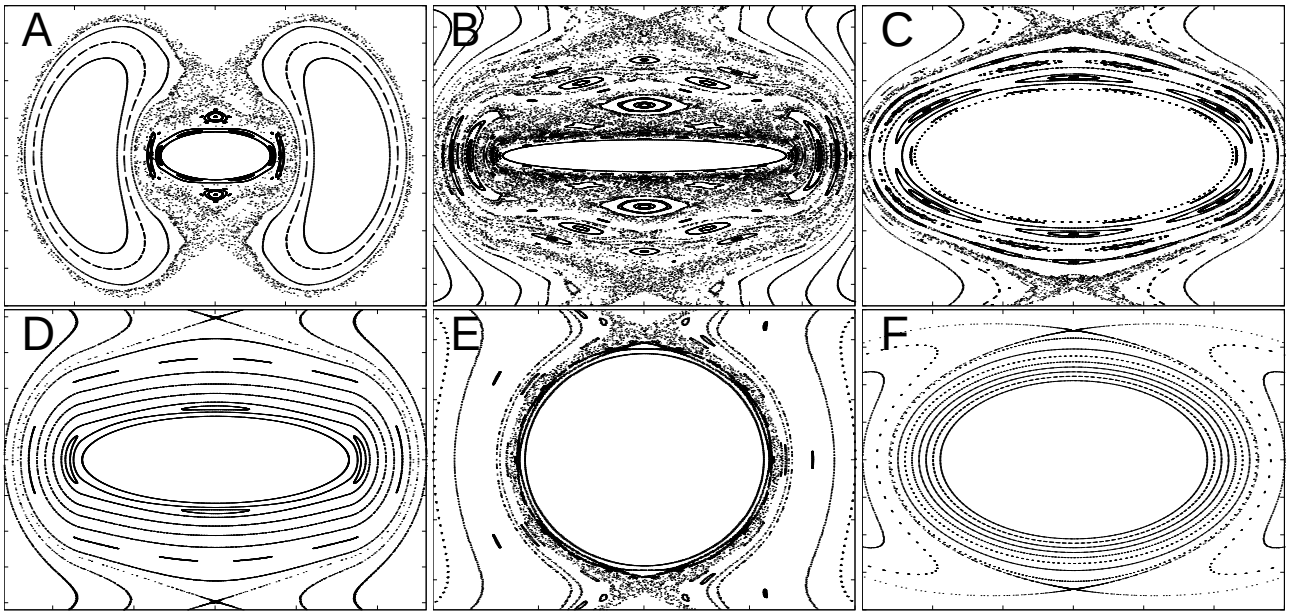

Figure 7: Poincaré surface of section in particle phase space (y, p). Plot A is with $(\eta, M) = (0.20, 0.30)$, Plot B (0.10, 0.15), Plot C (0.44, 0.25), Plot D (0.30, 0.10), Plot E (0.50, 0.60), Plot F (0.90, 0.10), corresponding, respectively, to Points A, B, C, D, E, F in Fig. 6. The last 5 are close-up plots, showing only up to the unstable fixed points and internal separatrices of the 2:1 resonance.

nances when they are outside the beam envelope; first the 10:3, followed by the 6:2, 8:3, 10:4, and then a chaotic layer going towards the 2:1 resonance. The resonances are separated by good tori and the instability growth rate should be small. Thus, this is the region on the edge of instability.

On the other hand, the Poincaré surface of section in Fig. 7D corresponding to Points D of Fig. 6 with $\eta = 0.30$ ($\kappa = 1.517$) and $M = 0.10$ shows the 6:2 resonance well separated from the 10:4 resonance with a wide area of good tori. Also the width of the 10:4 resonance is extremely narrow so that particles can hardly be trapped there. Unlike the situation in Figs. 7B and 7C, there is no chaotic region at the unstable fixed points and inner separatrices of the 2:1 resonance, making diffusion towards this resonance impossible. This region will be relatively stable.

Next consider the region with very large beam envelope mismatch like Points E of Fig. 6 with $\eta = 0.50$ ($\kappa = 0.75$) and $M = 0.60$. (The other Point E is at $R_{\max}/R_0 = 2.067$ and is therefore not visible in Fig. 6). The close-up Poincaré surface of section in Fig. 7E shows the beam envelope radius at $y = 0.566$ when $p_y = 0$. We can see that the unstable fixed points and the inner separatrices of the 2:1 resonance are very close by and are very chaotic. As soon as a particle diffuses out to $y = 0.62$, it reaches the chaotic sea and wanders towards the 2:1 resonance. Because the chaotic region is so close to the beam envelope, this region of large mismatch is also unstable, which is Gluckstern's region of instability at large mismatch.

Finally, we look at Points F of Fig. 6, which have small space charge $\kappa = 0.0106$ or $\eta = 0.90$ and small mismatch $M = 0.10$. The Poincaré surface of section is shown in Fig. 7F. The beam envelope is surrounded by good tori far away from the separatrices of the 2:1 resonance and no parametric resonances are seen. This is evident also from Fig. 6 that this region is not only free from primary resonances but also many higher-order resonances. The unstable fixed points and the separatrices of the 2:1 resonance are well-behaved and not chaotic. Thus, these points are very stable. If we keep the same space-charge perveance and increase the amount of envelope mismatch, we also do not see in the Poincaré surface of section any parametric resonances between the beam envelope and the separatrices for the 2:1 resonance. However, although the separatrices of the 2:1 resonance are not chaotic, they become closer and closer to the beam envelope. When the separatrices are too close, particles that are driven by a small perturbation away from the beam envelope will have a chance of traveling along the separatrices of the 2:1 resonance to form beam halo. From our discussions, it is clear that to avoid instability and halo formation, the beam should have small mismatch and be in a region that is far away from parametric resonances in the plane of mismatch and tune depression. The best solution for stability is certainly when the beam has small mismatch and small space-charge perveance.

The deep fissures of the (2,0) mode near $\eta = 4.7$ and 5.3 in Fig. 2 or 6 are probably the result of encountering the 10:3 and 6:2 parametric resonances. The width of the fissures should be related to the width of the resonance islands, which can be computed in the standard way. In general, a lower-order resonance island, like the 4:1, is much wider than a higher-order resonance island, like the 6:1.

We tried very hard to examine the region between the 4:1 and 10:3 resonances with a moderate amount of mismatch. We found this region very stable unless it is close to the 10:3 resonance. We could not, however, reproduce the slits that appear in Gluckstern's (4,0) mode.

6 ANGULAR MOMENTUM

Most K-V particles have nonzero angular momentum. When angular momentum is included in the discussion, we first extend the particle Hamiltonian of Eq. (4.12) in Floquet notations to both the x and y transverse planes:

$$\hat{H}_p = \frac{1}{2R^2}(\hat{x}^2+\hat{y}^2+\hat{p}_x^2+\hat{p}_y^2) + \kappa[\hat{x}^2+\hat{y}^2-\ln(\hat{x}^2+\hat{y}^2)]\,\Theta(\hat{x}^2+\hat{y}^2-1)\,. \quad (6.1)$$

It is preferable to use the circular coordinates $(\hat{r},\varphi)$ as independent variables; their canonical momenta are, respectively, $\hat{p}_r$ and $\hat{p}_\varphi$. The particle Hamiltonian becomes

$$\hat{H}_p = \frac{1}{2R^2}\left(\hat{r}^2+\hat{p}_r^2+\frac{\hat{p}_\varphi^2}{\hat{r}^2}\right)+\kappa(\hat{r}^2-\ln\,\hat{r}^2)\,\Theta(\hat{r}-1)\,, \quad (6.2)$$

where $\hat{r}^2=\hat{x}^2+\hat{y}^2$ and

$$\begin{pmatrix}\hat{p}_r\\ \hat{p}_\varphi/\hat{r}\end{pmatrix} = \begin{pmatrix}\cos\varphi & \sin\varphi\\ -\sin\varphi & \cos\varphi\end{pmatrix}\begin{pmatrix}\hat{p}_x\\ \hat{p}_y\end{pmatrix}\,. \quad (6.3)$$

Extending the generating function in Eq. (4.11) to include the x coordinates, it is straightforward to show

$$r=R\,\hat{r} \quad \text{and} \quad \hat{p}_\varphi=\hat{x}\hat{p}_y-\hat{y}\hat{p}_x=xp_y-yp_x\,. \quad (6.4)$$

Thus $\hat{p}_\varphi$ is the angular momentum of the particle, which is a constant of motion. Since it has the same functional form in both coordinate systems, its overhead accent $\hat{}$ will no longer be necessary. Particles belonging to the unperturbed K-V distribution are therefore subjected to the restriction

$$\hat{r}^2+\hat{p}_r^2+\frac{p_\varphi^2}{\hat{r}^2}=1\,, \quad (6.5)$$

from which we obtain

$$\hat{r}^2=\frac{1-\hat{p}_r^2}{2}+\left[\left(\frac{1-\hat{p}_r^2}{2}\right)^2-p_\varphi^2\right]^{1/2}\,. \quad (6.6)$$

Thus a K-V particle has an angular momentum restricted by

$$|p_\varphi|\le\frac{|1-\hat{p}_r^2|}{2}\le\frac{1}{2}\,, \quad (6.7)$$

which agrees with the result of Riabko [6] that $2J_r+|p_\varphi|=\frac{1}{2}$, where J_r is the radial action. The equation of motion for the particle radial position inside the beam core is

$$\frac{d^2\hat{r}}{d\psi^2}+\hat{r}-\frac{p_\varphi^2}{\hat{r}^3}=0\,, \quad (6.8)$$

where the Floquet phase advance $d\psi = d\theta/R^2$ has been used. Notice that this is exactly the same as the envelope equation in Eq (4.7) with $\kappa=0$. We proved in Sec. 2 that the envelope tune is exactly twice the particle tune when $\kappa\to 0$. Hence, comparing with the equation of motion of a zero-angular-momentum particle in the presence of a mismatched space-charge dominated beam, i.e., Eq. (4.10), we can conclude that the particle radial tune inside the beam core is exactly twice the zero-angular-momentum particle tune for any space charge and mismatch.

Simulations have been performed for the time evolution of the radial motion of a beam particle and then compared with the time evolution of the transverse motion of a particle with zero momentum. One of the simulations is shown in the upper plot of Fig. 8. The particle is a K-V particle with angular momentum $p_\varphi=0.3$ satisfying the K-V restriction of Eq. (6.6) in a mismatched beam envelope with $M=0.30$ having a tune depression of $\eta=0.23$. We see that the shape of oscillations of r shown as solid is very similar to that of y with zero angular momentum shown as dashes. Since r does not go negative, its tune appears to be twice the tune of a zero-angular-momentum particle. This plot was performed near a 6:1 resonance for a zero-angular-momentum particle and it therefore translates into a 3:1 resonance for a nonzero-angular-momentum particle.

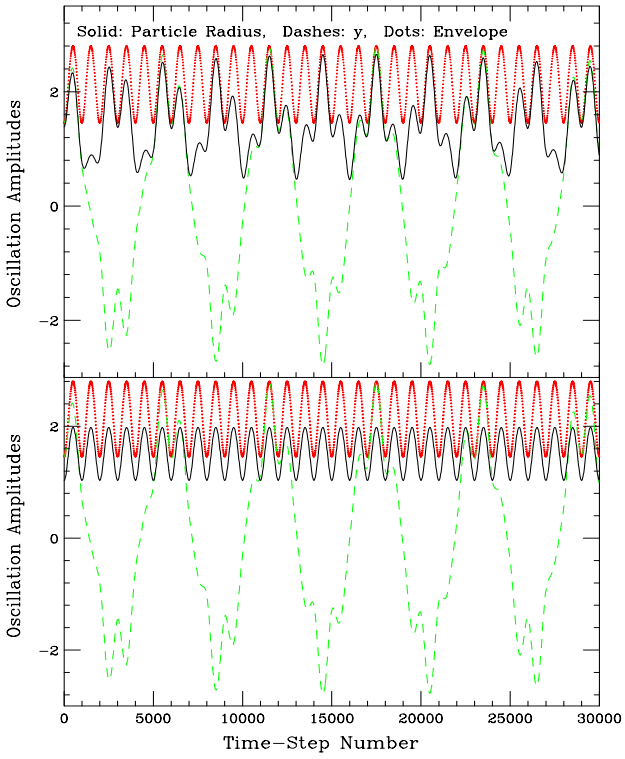

Figure 8: Plots showing the time evolution of the radial position r of a K-V particle in solid inside a beam envelope with nonzero p_φ, mismatch $M=0.30$ and $\kappa=2.059$ ($\eta=0.23$). The evolution y of a $p_\varphi=0$ particle is shown in dashes. The simulation is at the 6:1 resonance for the $p_\varphi=0$ particle. Top plot shows the radial motion with $p_\varphi=0.30$ which is twice as fast as the oscillating motion of a $p_\varphi=0$ particle. Lower plot is for $p_\varphi=0.50$. Now the particle radius r is related to the envelope radius R by $r=\sqrt{|p_\varphi|}R=R/\sqrt{2}$, giving a false impression that the radial tune becomes equal to the envelope tune.

It is interesting to point out that as $|p_\varphi|\to\frac{1}{2}$, the humps that exhibit in the time evolution of the radial motion become more pronounced and the time evolution eventually becomes proportional to the envelope oscillation, as is demonstrated in lower plot of Fig. 8. Now the radial tune appears to change suddenly to the envelope tune instead. In fact, this is easy to understand. The equation of motion for the particle radial position is

$$r''+r=\frac{2\kappa}{R^2}r+\frac{p_\varphi}{r^3}\,. \quad (6.9)$$

Compared with the envelope equation (4.7), it is evident that $r=\sqrt{|p_\varphi|}R$ is a solution. In the Floquet representation, Eq. (6.8) also reflects such a solution. Thus, it is apparent that the radial tune can assume two different val-

ues. This ambiguity can be resolved by investigating the Poincaré surface of section of the radial motion. In the Floquet coordinates, the trajectory is represented by one point, $\hat{r} = \sqrt{|p_\varphi|}$ and $\hat{p}_r = 0$. In the (r, p_r) coordinates, the Poincaré surface of section is also a single point since the phase-space position of the particle is plotted only every envelope period. In fact, from Eq. (6.2), the Hamiltonian in the Floquet representation, it is clear that the solution $\hat{r} = \sqrt{|p_\varphi|}$ is the lowest point of the radial potential. This is the equilibrium solution which, in the case of a Hill's equation, is equivalent to a particle traveling along an orbit passing through the centers of all elements. Therefore, even in this solution, the radial tune is *not* equal to the envelope tune, but remains twice the tune in the Cartesian coordinates.

Because of the above discussion, all the n:m parametric resonances that we studied in Sec. 5 just translate into the $\frac{n}{2}$:m resonances in a r-p_r Poincaré surface of section. As a result, the stability investigation in the previous section should hold even when particles with finite angular momentum are included.

7 CONCLUSIONS

We have now an interpretation of the collective instabilities in the plane of envelope mismatch and tune depression through the particle-beam nonlinear-dynamics approach. Because of the existence of noises of all types in the accelerators and the K-V equation is far from realistic, some particles will diffuse away from the K-V distribution. Although these particles may encounter parametric resonances once outside the beam core, an equilibrium will be reached if these resonances are bounded by invariant tori. It may happen that the island chains outside the beam envelope are so close together that they overlap to form a chaotic sea. When the last invariant torus breaks up, particles leaking out from the core diffuse towards the 2:1 resonance, which is usually much farther away from the beam envelope, to form beam halos. As particles escape from the beam envelope, the beam intensity inside the envelope becomes smaller and the equilibrium radius of the beam core shrinks. Thus more particles will find themselves outside the envelope. As this process continues because no equilibrium can be reached, the beam eventually becomes unstable.

It is possible that many collective instabilities can be explained by the particle-beam nonlinear-dynamics approach. The wakefields of the beam interacting with the particle distribution produce parametric resonances and chaotic regions. Instabilities will be the result of particles trapped inside these resonance islands. The perturbed bunch structure further enhances the wakefields to induce these collective instabilities of the whole beam.

So far, we have been able to explain the results of Gluckstern, *et. al* qualitatively. However, there are differences quantitatively. To the lowest order, the Vlasov equation studied by Gluckstern, *et. al.* does involve the perturbation force induced by the *perturbation* distribution via the Poisson's equation. In our nonlinear-dynamics approach, the particle that escapes from the beam envelope core, always sees the Coulomb force of the *entire unperturbed beam core*, independent of any variation of the core distribution due to the leakage of particles. This is due to the fact that the envelope Hamiltonian and the particle Hamiltonian have been treated separately. This leads to a dependency of the particle equation of motion on the envelope radius, but not the dependency of the equation of motion of the envelope radius on the particle motion. We believe that this is the reason why we have not been able to compute the growth rates of the instabilities. However, an improvement of the present model is nontrivial. This is not the problem of one particle interacting with a beam core in such a way that the perturbation of the beam core can be neglected, because a beam core that is not modified cannot lead to instability of any form. To treat the problem properly, the Hamiltonian will have to include undoubtedly all the beam particles interacting with each other, from which the time evolution of the beam core is to be determined. This appears to be a very complex problem, and this is exactly why the Vlasov equation is introduced. The Vlasov equation is a time-dependent differential equation of the beam core or beam distribution and requires only the single-particle Hamiltonian. Thus, it appears that the Vlasov equation will be unnecessary only when the beam particle distribution does not play an essential role, for example, in the issues of Robinson instability, the two-particle strong head-tail instability, the two-particle chromaticity-driven head-tail instability, etc.

8 REFERENCES

[1] I.M. Kapchinskij and V.V. Vladimirskij, Proc. Int. Conf. on High Energy Accelerators, CERN, Geneva, 1959, p.274.

[2] D.D. Caussyn, *et. al.*, Phys. Rev. **A46**, 7942 (1992); M. Ellison, *et. al.*, Phys. Rev. Lett. **70**, 591 (1993); M. Syphers, *et. al.*, Phys. Rev. Lett. **71**, 720 (1993); D. Li, *et. al.*, Phys. Rev. **E48**, R1638 (1993); DD. Li, *et. al.*, Phys. Rev. **E48**, 3 (1993); H. Huang, *et. al.*, Phys. Rev. **E48**, 4678 (1993); Y. Wang, *et. al.*, Phys. Rev. **E49**, 1610 (1994); Y. Wang, *et. al.*, Phys. Rev. **E49**, 5697 (1994); S.Y. Lee, *et. al.*, Phys. Rev˙**E49**, 5717 (1994); M. Ellison, *et. al.*, Phys. Rev. **E50**, 4051 (1994); L.Y. Liu, *et. al.*, Phys. Rev. **E50**, R3344 (1994); D. Li, *et. al.*, Nucl Inst. Meth. **A364**, 205 (1995).

[3] E. Keil and W. Schnell, CERN Report SI/BR/72-5, 1972; D. Boussard, CERN Report Lab II/RF/Int./75-2, 1975.

[4] K.Y. Ng and S.Y. Lee, "Particle-Beam Approach to Collective Instabilities—Application to Space-Charge Dominated Beams," Proc. 16th Advanced ICFA Beam Dynamics Workshop on Nonlinear and Collective Phenomena in Beam Physics, Arcidosso, Sep. 1-5, 1998.

[5] S.Y. Lee and A. Riabko, Phys. Rev. **E51**, 1609 (1995).

[6] Riabko, A., Ellison, M., Kang, X., Lee, S.Y., Li, D., Liu, J.Y., Pei, X., and Wang, L., *Phys. Rev.* **E51**, 3529 (1995).

[7] R.L. Gluckstern, W-H. Cheng, and H. Ye, Phys. Rev. Lett. **75**, 2835 (1995); R.L. Gluckstern, W-H. Cheng, S.S. Kurennoy, and H. Ye, Phys. Rev. **E54**, 6788 (1996).

[8] In Ref. 6, the section on Mathieu instability and stop-band is incorrect.

[9] Forest, E. and Berz, M., LBL Report LBL-25609, ESG-46, 1989.